NINETEENTH EUROPEAN ROTORCRAFT FORUM

Paper n° C 16

COMPRESSIBLE NAVIER-STOKES COMPUTATIONS OF DYNAMIC STALL

by

DONG-HO LEE and CHAN-JIN NAM

DEPT. OF AEROSPACE ENGINEERING

SEOUL NATIONAL UNIVERSITY

SEOUL, KOREA

September 14- 16, 1993

CERNOBBIO (Como)

ITALY

ASSOCIAZIONE INDUSTRIE AEROSPAZIALI

ASSOCIAZIONE ITALIANA DI AERONAUTICA ED ASTRONAUTICA

COMPRESSIBLE NAVIER-STOKES COMPUTATIONS OF DYNAMIC STALL

Dong-ho Lee*, Chan-jin Nam**
Department of Aerospace Engineering
Seoul National University, Seoul, Korea

Abstract - The unsteady flowfields around an oscillating airfoil are analyzed by solving the two-dimensional compressible Navier-Stokes equations with a moving grid. An upwind biased flux-difference-splitting (FDS) of Roe and ADI method with Newton subiteration are used to solve the equations. The formation and convection of vortex structures and details of the dynamic stall phenomenon have been calculated. The computed unsteady aerodynamic loads agree well with the experimental data. A substantial reduction in computer time to resolve a pitching motion is obtained by using larger time steps with no loss in temporal accuracy. The simultaneous velocity and pitch oscillations are also considered for a proper simulation of complex motion of the helicopter rotor blade in forward-flight. The effects of combined motion on the aerodynamic loads are investigated.

I. Introduction

Dynamic stall refers to the complex series of events that result in dynamic delay of stall, on airfoils and wings experiencing unsteady motion, to angles significantly beyond the static-stall angle[1]. During high speed forward flight of helicopter, due to the large flapping motion of the blade, some blade sections have periodically very large angle of attack on the retreating side. As a result dynamic stall occurs, and it causes a significant increase in the blade stress and the control system loads. Thus, the dynamic stall constitutes a major limiting factor for the helicopter flight envelope[2].

During the last 20 years, many studies of dynamic stall have been made[1]. However, a complete understanding of these complex unsteady effects has not been achieved, and there is a great need for fundamental studies. The difficulty mainly arise because these flows are extremely complex and are not amenable to standard experimental and numerical techniques. McCroskey et al [3] performed an extensive experiment on dynamic stall on pitching airfoil sections. Many numerical studies by solving incompressible Navier-Stokes equations for laminar flow were performed[4,5]. The tip mach number of the retreating blade can be very low, but it was found that the local flow around the leading edge can become supersonic even if the Mach number increases beyond 0.2 [1]. It was also shown that compressibility can introduce a significant effect on dynamic stall [6]. Relatively recently, a few numerical studies have been performed by solving the compressible Navier-Stokes equations [7,8,9]. In these studies, the Beam & Warming's ADI algorithm[10] which is a central difference method, and needs an addition of artificial dissipation term for stability was used. This algorithm, where the time step size is limited by linearization and factorization error, may require more than 10,000 time steps for a single cycle of unsteady motion.

This paper presents an efficient and accurate method for computing the massively separated unsteady turbulent flowfields in the moving domain and shows some computational results of the dynamic stall. The governing equations of flow are compressible Navier-Stokes equations in moving mesh. A finite-volume upwind-biased algorithm of Roe[11] is adopted to overcome the limitations of the central difference scheme. The AF-ADI method of Beam & Warming and Newton subiteration[12] are used for time integration. The Newton subiteration has proven to be effective in reducing the computational work by reducing the linearization and factorization errors of implicit operator while maintaining time accuracy.

The histories of aerodynamic loads such as lift, drag and pitching moment are evaluated and compared with experimental data. The detailed vortex patterns, vorticity distribution, surface pressure and shear stress are investigated.

For a more proper simulation of the complex environment of rotors in forward flight, a dynamic

---

* Professor
** Graduate Assistant

stall due to simultaneous fluctuations in velocity and pitch angle[13] are also computed and the effect of the combined motion on the histories of aerodynamic loads and vortex structures are investigated.

II. Compressible Navier-Stokes Equations

The governing partial differential equations under consideration are the two dimensional unsteady, compressible, full Navier-Stokes Equations in moving grid domain. These equations are transformed from the Cartesian reference frame (t, x, y) to the arbitrary curvilinear coordinate (τ, ξ, η) where ξ and η are along the chordwise and normal directions of airfoil, respectively. The transformed equations written in conservation-law form are given by

$$\frac{\partial \hat{Q}}{\partial \tau} + \frac{\partial \hat{E}}{\partial \xi} + \frac{\partial \hat{F}}{\partial \eta} = \frac{1}{\mathrm{Re}_a}\left(\frac{\partial \hat{E}_v}{\partial \xi} + \frac{\partial \hat{F}_v}{\partial \eta}\right) \tag{1}$$

where the vector of conserved variables $\hat{Q}$ and fluxes are given by

$$\hat{Q} = \frac{1}{J}\begin{bmatrix}\rho\\ \rho u\\ \rho v\\ e\end{bmatrix}, \quad \hat{E} = \frac{1}{J}\begin{bmatrix}\rho U\\ \rho u U + p\xi_x\\ \rho v U + p\xi_y\\ (e+p)U - \xi_t p\end{bmatrix}, \quad \hat{E}_v = \frac{1}{J}\begin{bmatrix}0\\ \xi_x\tau_{xx} + \xi_y\tau_{yx}\\ \xi_x\tau_{xy} + \xi_y\tau_{yy}\\ (\hat{e}_v)_4\end{bmatrix}$$

$$(\hat{e}_v)_4 = u(\xi_x\tau_{xx} + \xi_y\tau_{yx}) + v(\xi_x\tau_{xy} + \xi_y\tau_{yy}) + \kappa\left(\xi_x\frac{\partial T}{\partial x} + \xi_y\frac{\partial T}{\partial y}\right)$$

The contravariant velocities U and V are defined by

$$U = \xi_t + \xi_x u + \xi_y v = \xi_x(u - x_\tau) + \xi_y(v - y_\tau), \quad V = \eta_t + \eta_x u + \eta_y v = \eta_x(u - x_\tau) + \eta_y(v - y_\tau) \tag{2}$$

where x_τ and y_τ are the grid speeds in the x and y directions, respectively, and the pressure p is given by the equation of state for a perfect gas

$$p = (\gamma - 1)[e - \rho(u^2 + v^2)/2] \tag{3}$$

These equations have been nondimensionalized by chord length and free stream values.

III. Numerical Procedure

Spatial Differencing

In the present study, a finite-volume upwind-biased flux-difference-splitting algorithm of Roe and Beam & Warming's ADI method are used for computing the flows around moving airfoils. The upwind discretizations such as flux-vector splitting (FVS) of van Leer[14] and flux-difference splitting (FDS) of Roe account for the local wave propagation characteristics of the flow and they can capture shock waves sharply. One of the most important advantages of the upwind difference is that these discretizations are naturally dissipative and consequently do not require additional artificial dissipation terms or adjustment of free parameters to control the dissipation. The FDS of Roe has less dissipation than the FVS of van Leer and can produce more accurate results for viscous computations[12].

In Roe's approach, the flux difference between two neighbouring states at the cell interface is divided into component parts associated with each wave speed. The numerical normal flux

component of Roe at the cell can be written for the ξ direction as

$$\hat{E}_{i+\frac{1}{2}} = \frac{1}{2}[\hat{E}(Q_L) + \hat{E}(Q_R) - |\tilde{A}(Q_L,Q_R)|(Q_R - Q_L)] \tag{4}$$

where $\tilde{A}$ is the Jacobian matrix with the Roe-averaged values and $|\tilde{A}|(Q_R - Q_L)$ the dissipation term contributions to the interface flux.

The Q_L and Q_R are the state variables to the left and right of the cell interface. The time metrics for the grid motion are included in this evolution. The state variable at the interface is constructed from nonoscillatory interpolation of primitive variables $q = (\rho, u, u, v, p)$ where high-order accurate differencing is given by one-parameter family

$$q_L = q_i + \frac{s}{4}[(1-\kappa)\nabla_i + (1+\kappa)\Delta_i] \quad , \quad q_R = q_{i+1} - \frac{s}{4}[(1+\kappa)\nabla_{i+1} + (1-\kappa)\Delta_{i+1}] \tag{5}$$

where ∇ and Δ are backward and forward difference of q, respectively, that are limited using Koren's differentiable limiter to ensure the monotone interpolation across discontinuities in the solution[15]. The parameter κ in Eq. (5) controls a family of difference schemes by appropriately weighting ∇ and Δ. For all of the results presented, κ = 1/3 was used for the third-order discretization.

The viscous flux terms are discretized using standard second-order central differencing.

Implicit Temporal Discretization

The AF-ADI method of Beam & Warming and Newton subiteration are used in the present study of time integration. The AF-ADI method in two dimensions is unconditionally stable and thus allows the selection of the time step size based on the temporal accuracy be dictated by the problem being considered, rather than on the numerical stability of the algorithm. Consequently, an appropriate time step may be selected for the unsteady problem. This time step however, may still be relatively small so that resolving the motion requires extensive computational effort, especially for viscous flow where very dense grids are used. And the accumulations of linearization and factorization errors due to large time step can degrade the temporal accuracy for unsteady flows. The Newton subiteration method has proven to be effective in reducing the computational work by reducing above errors while maintaining the time accuracy.

With three point backward Euler time integration, a second order time accurate scheme for Eq.(1) can be written as

$$\left[\frac{I}{J} + \frac{2}{3}\Delta\tau\frac{\partial R}{\partial Q}\right]^n \Delta Q^n = -\frac{2}{3}\Delta\tau R^n(1) + \frac{1}{3J}\Delta Q^{n-1} \tag{6}$$

where R is the steady state terms of Eq. (1) and $\partial R/\partial Q$ the Jacobian of flux vectors. The residual is computed using FDS of Roe, but the exact Jacobian of FDS is too expensive to compute and thus the Jacobians of van Leer flux[14] are used in the LHS(6). The Jacobian of viscous flux in η direction is included.

The implementation of subiterations into the scheme described by Eq. (6) is a simple additional term added to the right hand side and a redefinition of ΔQ^n on the LHS(6).

$$\left[\frac{I}{J} + \frac{2}{3}\Delta\tau\frac{\partial R}{\partial Q}\right]^n \Delta Q^p = -\frac{2}{3}\Delta\tau R^p(1) + \frac{1}{J}(Q^p - \frac{4}{3}Q^n + \frac{1}{3}Q^{n-1}) \tag{7}$$

where ΔQ^p is defined as $\Delta Q^{p+1} - \Delta Q^p$ and p is the subiteration count. In general, p decreases as $\Delta\tau$ is reduced. At convergence, $Q^p = Q^{n+1}$. When p=0, $Q^p = Q^n$, and the system reverts to the noniterative scheme.

All boundary conditions except the wall condition are applied explicitly and the mean free stream

conditions are used for initial conditions.

Dynamic Grid Generation

The initial grid was generated by using conformal maping method [16]. A 161×41 C-type grid which has fine clustering to the body surface in the normal direction was used to resolve the viscous zone (Fig.1). The normal distances of the first grid points at the surface are less than 0.00001C. The grid system is attached to the airfoil and has rigid body motions with the airfoil. The origin of the coordinate is located at quarter chord. The dynamic grid for a pitching airfoil can be presented as

$$x^{n+1} = cos(\Delta\alpha)x^n + sin(\Delta\alpha)y^n \ , \ y^{n+1} = -sin(\Delta\alpha)x^n + cos(\Delta\alpha)y^n \tag{8}$$

$$x_\tau^{n+1} = \dot{\alpha}y^{n+1} \ , \ y_\tau^{n+1} = -\dot{\alpha}x^{n+1} \tag{9}$$

The fluctuation component of the free stream velocity in combine dynamic stall is included in the grid velocity x_τ.

IV. Numerical Results and Discussion

For the validation of the developed code, this flow solver was extensively used to calculate unsteady flows such as small pitch oscillation, plunging motion, and translational motion of airfoil[17]. The results show good agreements with unsteady experimental data or other numerical results even for calculations using large Courant number (order of $10^3 - 10^4$) with only 2 or 3 sub-iterations. This Newton sub-iterative procedure reduced the errors of factorization and linearization, so that larger time steps can be used and substantial reduction in computer time is obtained with no loss in accuracy. The effects of implicit boundary condition and viscous Jacobian on stability and convergency have been investigated. Turbulent viscosity is evaluated using the Baldwin-Lomax algebraic model[18]. Wu et al. [8] and Rizzetta et al. [19] showed that no clear trend could be found favoring the use of higher-order turbulence models in massively separated flows.

Dynamic Stall Due to Pitch Oscillation

The unsteady flowfield around a NACA0012 airfoil oscillating in pitch about its quarter chord has been investigated. The pitching motion is

$$\alpha = \alpha_0 + \alpha_m sin(2M_\infty k\tau) \ , \ \alpha_0 = 15^o \ , \ \alpha_m = 10^o \ , \ k = 0.151 \tag{10}$$

where α_0 and α_m are the mean and amplitude of angle of attack, and k is the reduced frequency defined as $\omega c/2U_\infty$. The freestream Mach number, Reynolds number $U_\infty c/\nu$ and period (2 phi)/(2 M sub inf k) were 0.283, 3.45×10^6 and 73.517, respectively.

When $\Delta\tau$ is 0.05, a stable and time step independent solution was obtained with two subiterations. Each cycle of oscillation required about 1500 time steps and 3000 subiterations (total 4500 iterations). Wu et al. [7] needed 14000 time steps per cycle, therefore we can save about two thirds of the computer time. It was also verified that the viscous Jacobian and the implicit treatment of the wall boundary condition enhanced the convergency with respect to subiteration at each time level. It was shown that a little modification to the turbulent model and the transition model can change the incipient of separation and development of a dynamic stall vortex.

The development of unsteady flowfields is shown in Fig. 2. in terms of instantaneous streamlines and iso-vorticity contours. The pitching airfoil passes the static angle(about 13°) without any discernible change in the viscous or inviscid flow around the airfoil. However, boundary layer on the upper surface grow considerably. A separation of the boundary layer near the leading edge and the development of the leading+ edge vortex is observed at $\alpha = 20^o$. During the upstroke, the primary

leading edge vortex moves along the surface and continues to grow. In the meantime, the shear layer vortex at the upper surface near the trailing edge increases the shedding of reversed lower surface vorticity from the trailing edge. The shear layer vortex interacts with this reversed trailing edge vortex so that a pair of counter rotating vortices is formed at the trailing edge($\alpha = 25^o$). During the downstroke, the leading edge vortex moves away from the airfoil and shed into the wake, and the trailing counter rotating trailing edge vortex is increased($\alpha = 24^o$). At $\alpha = 23.29^o$, the trailing edge vortex also sheds into the wake. Some weak vortices are subsequently developed and convect downstream. The flow reattachment process starts from the leading edge to the downstream as α decreases.

Fig. 3 shows the aerodynamic loads on the airfoil. The present computation predicts lower lift and drag during the upstroke. At $\alpha = 24^o$, as a result of shedding of leading edge vortex, the lift drops drastically. The delay of leading edge vortex shedding and overprediction of the trailing edge vortex suction during the downstroke can be attributed to the turbulence model. It was shown that the Baldwin - Lomax model produce less diffusion than that was observed physically, so that stall is delayed[19].

The instantaneous surface pressures are shown in Fig. 4. The critical pressure coefficient for $M_\infty = 0.283$ is -7.875. The surface pressure shows that the local flow around the leading edge becomes supersonic. If a shock appears, it could dramatically affect the dynamic stall process, but no evidence of shock is found. After the leading edge vortex is developed, vortex induced suction peaks are shown. Fig. 5 represents the upper surface shear stress distributions.

Dynamic Stall Due to Combined Motion

For a proper simulation of dynamic stall of the helicopter rotor blade section in forward flight, a simultaneous velocity and angle of attack fluctuations are comsidered. The air velocity with respect to the blade airfoil during forward flight of the helicopter is high at the advancing side and low at the retreating side, but by flapping motion, the angle of attack is low at advancing side and vice versa.

Only a out-of-phase motion is consdered :

$$\alpha = \alpha_0 + \alpha_m sin(2M_0 k\tau) \ , \ \alpha_0 = 15^o \ , \ \alpha_m = 10^o$$

$$M_t = M_0 - M_m sin(2M_0 k\tau) \ , \ M_0 = 0.283 \ , \ M_m = 0.170 \ , \ k = 0.151 \ , \ Re = 3.45 \times 10^6 \qquad (11)$$

The fluctuation component of velocity, $-M_m sin(2M_0 k\tau)$, is included in x_τ so that $x_\tau = \dot{\alpha} y^{n+1} + M_m sin(2M_0 k\tau)$.

The two aerodynamic coefficients defined with respect to the free stream velocity relative to airfoil and mean velocity are compared.

$$C_{L,0} = \frac{Lift}{0.5\gamma p_\infty (M_o)^2} \ , \quad C_{L,t} = \frac{Lift}{0.5\gamma p_\infty (M_t)^2} \qquad (12)$$

Fig. 6 shows the aerodynamic loads history of combined motion. The $C_{L,t}$ begins to rise faster with increasing incidence than before so that dynamic $C_{L,t}$ overshoot is increased compared to dynamic stall of pitching airfoil. The lift stall angle is also increased. These are the characteristics of dynamic stall in low Mach number[1]. The $C_{L,0}$ which means the lift over mean dynamic pressure produces no peak at high incidence. The drag and pitching moment have similar patterns compared to lift.

Therefore, the out-of-phase motion of velocity and angle of attack reduced the peaks in the histories of the unsteady aerodynamic loads during the dynamic stall process. The aerodynamic load coefficients defined with respect to the velocity relative to the airfoil show the similar histories compared to the those of dynamic stall by the pitching motion.

V. Conclusion

The unsteady flowfields around a pitch oscillating and a pitch/velocity oscillating NACA0012 airfoil are analyzed by solving the two-dimensional compressible Navier-Stokes equations with a moving grid. The inviscid flux terms are computed by using an upwind biased flux-difference-splitting (FDS) of Roe. For temporal discretization, ADI method with Newton subiteration are used.

By reducing the linearization and factorization errors of implicit operator by Newton subiteration, a large time step can be used without degrading the temporal accuracy for dynamic stall. A substantial reduction in computer time, about two thirds of total time steps was accomplished, to resolve a pitching motion with no loss in temporal accuracy.

The process of dynamic stall, such as the formation and convection of the leading edge vortex and details of the dynamic stall phenomenon have been investigated. The computed unsteady aerodynamic loads agree well with the experimental data. But the poor performance of the turbulence model at high angle of attack and in the wake region delayed the leading edge vortex shedding and overpredicted the trailing edge vortex suction during the downstroke. During the upstroke, the computed surface pressure shows that the local flow around the leading edge becomes supersonic.

The simultaneous velocity and pitch oscillations in out-of-phase motion are also considered for a proper simulation of complex motion of helicopter rotor blade in forward-flight. The combined motion reduced the peaks in the histories of the unsteady aerodynamic loads during the dynamic stall process. The aerodynamic load coefficients defined with respect to the velocity relative to the airfoil show the similar histories compared to the those of dynamic stall by the pitching motion.

Reference

1. L. W. Carr, Progress in Analysis and Prediction of Dynamic Stall, Journal of Aircraft, Vol. 25, No. 1, Jan. 1988, pp. 6-17.
2. S.T. Gangwani, Prediction of Dynamic Stall and Unsteady Airloads for Rotor Baldes, Journal of American Helicopter Society, Oct. 1982, pp.57-64.
3. W. J. McCroskey, K. W. McAlister, L. W. Carr, and S. L. Pucci, An Experimental Study of Dynamic Stall in Advanced Airfoil Sections, NASA TM 84245, Vol.1-3,, July 1982.
4. I. H. Tuncer, J. C. Wu, and C. M. Wang, Theoretical and Numerical Studies of Oscillating Airfoils, AIAA Journal, Vol. 28, No. 9, Sept. 1990, pp. 1615-1624.
5 C. Shih, L. Lourenco, L. van Dommelen, and A. Krothapalli, Unsteady Flow Past an Airfoil Pitching at a Constant Rate, AIAA Journal, Vol. 30, No. 5, May 1992, pp.1153-1161.
6. M. S. Chandrasekhara, L. W. Carr, Flow Visulation Studies of Mach Number Effects on Dynamic Stall of an Oscillating Airfoil, Journal of Aircraft, Vol. 27, No. 6, June 1990, pp. 516-523.
7. J. Wu, K.R.V. Kaza, and L.N. Sankar, Technique for the Prediction of Airfoil Flutter Characteristics in Separated Flow, Journal of Aircraft, Vol. 25, No. 2, Febr. 1989, pp. 168-177.
8. J. C. Wu, D. L. Huff, L. N. Sankar, Evaluation of Three Turbulence Models in Static Air Loads and Dynamic Stall Predictions, Journal of Aircraft, Vol. 27, No. 4, April 1990, pp. 382-384
9. M. R. Visbal, Dynamic Stall of a Constant-Rate Pitching Airfoil, Journal of Aircraft, Vol. 27, No. 5, May 1990. pp.400-407.
10. J. Steger, Implicit Finite-Difference Simulation of Flow about Arbitrary Two-Dimesional Geometrics, AIAA Journal, Vol. 16, No. 4, 1978, pp. 679-686.
11. P. L. Roe, Approximate Riemann Solvers, Parameter Vectors, and Difference Schemes, Journal of Computational Physics, Vol.43, No.3, 1981, pp.357-372.
12. B. Simpson, Unsteady Three Dimensional Thin Layer Navier-Stokes Solutions on Dynamic Blocked Grids, Ph.D Dissertation, Mississippi University, 1988.
13. D. Favier, A. Agnes, C. Barbi, and C. Maresca, Combined Translation/Pitch Motion: A New Airfoil Dynamic Stall Simulation, Journal of Aircraft, Vol. 25, No. 9, Sept. 1988, pp.805-814.
14. W. K. Anderson, J. L. Thomas, and B. van Leer, Comparision of Finite Volume Flux Vector

Splittings for the Euler Equations, AIAA Journal, Vol. 24, No. 9, Sept. 1986, pp. 1453-1460.
15. C. L. Chen, W. J. McCroskey, and S. Obyashi, Numerical Solutions f Forward-Flight Rotor Flow Using and Upwind Method, Journal of Aircraft, Vol. 28, No. 6, June 1991, pp. 374-380.
16. K. Inoue, Grid Generation for Single Airfoil using Conformal Mapping, NAL TR-851T.
17. C. J. Nam, Navier-Stokes Computations of Dynamic Stall and BERP blade Flowfields, Ph.D. Dissertation, Seoul Nat'l University, Aug. 1993.
18. B. S. Baldwin, H. Lomax, Thin Layer Approximation and Algebraic Model for Separated Turbulent Flows, AIAA Paper 78-0257, Jan. 1978.
19. D. P. Rizzetta, M. R. Visbal, Comparative Numerical Study of Two Turbulence Models for Airfoil Static and Dynamic Stall, AIAA Journal, Vol. 31, No. 4, pp. 784-786.

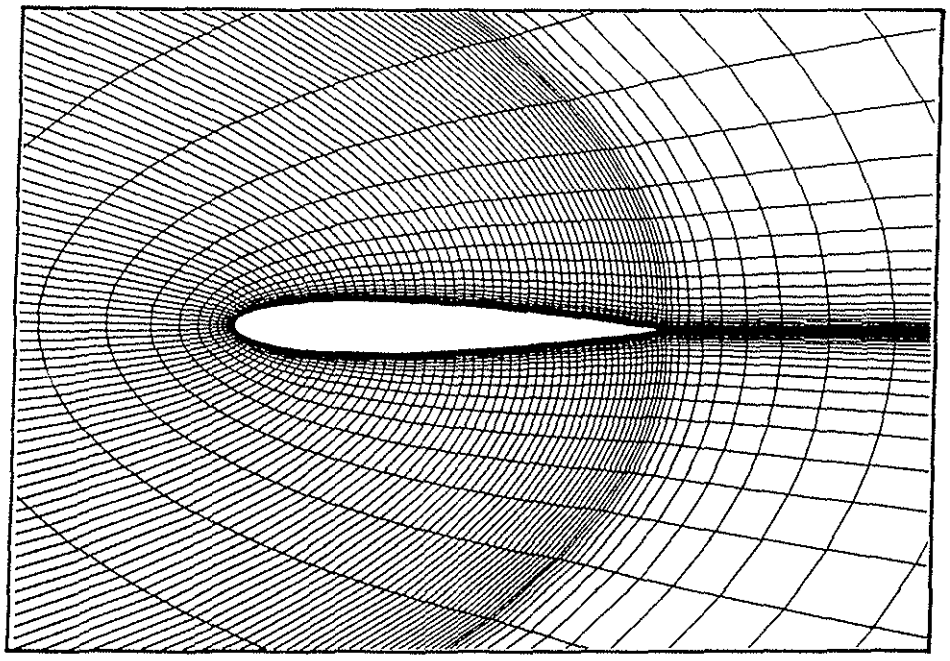

Fig. 1 Computational Grid(161×41)

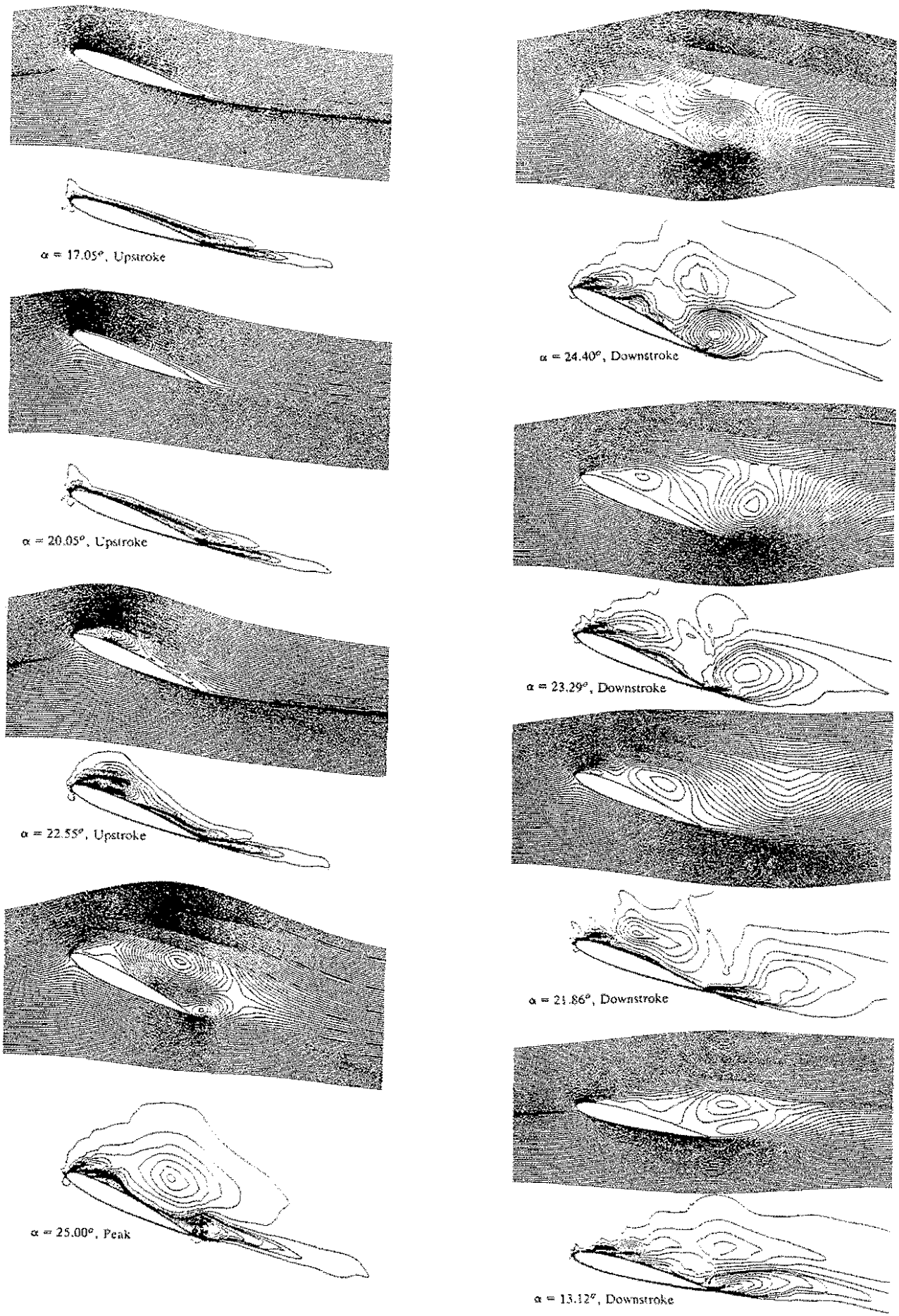

Fig. 2 Instantaneous Streamlines and Iso-vorticity Contours
NACA0012, $M_\infty = 0.283$, $\mathrm{Re} = 3.45 \times 10^6$, $\alpha = \alpha_0 + \alpha_m \sin(2M_\infty k\tau)$, $\alpha_0 = 15^o$, $\alpha_m = 10^o$, $k = 0.151$

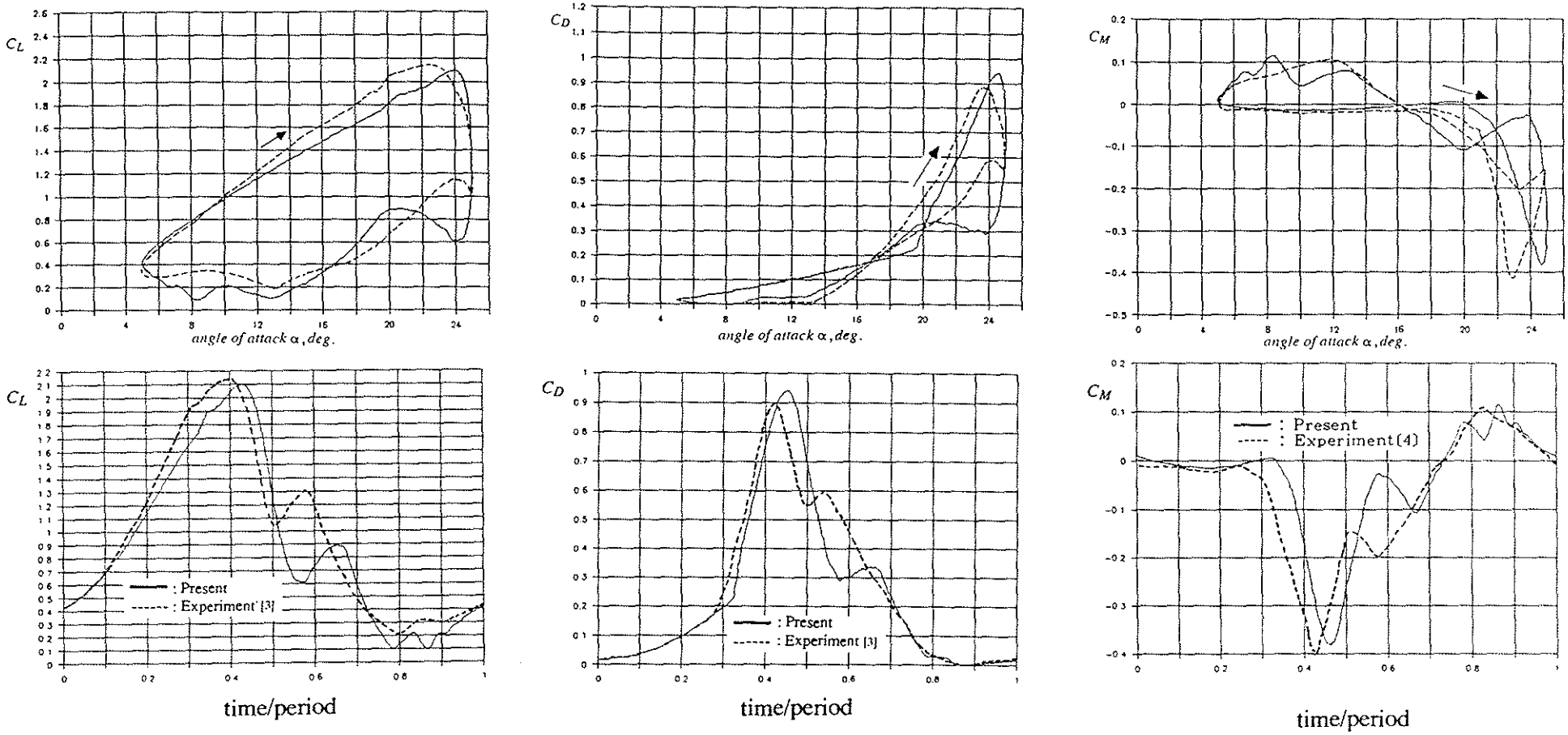

(a) Lift (b) Drag (c) Pitching Moment

Fig. 3 Comparision of Present and Experimental Aerodynamic Loads Coefficient
NACA0012, $M_\infty = 0.283$, $\mathrm{Re} = 3.45\times10^6$, $\alpha = \alpha_0 + \alpha_m \sin(2M_\infty k\tau)$, $\alpha_0 = 15^o$, $\alpha_m = 10^o$, k=0.151

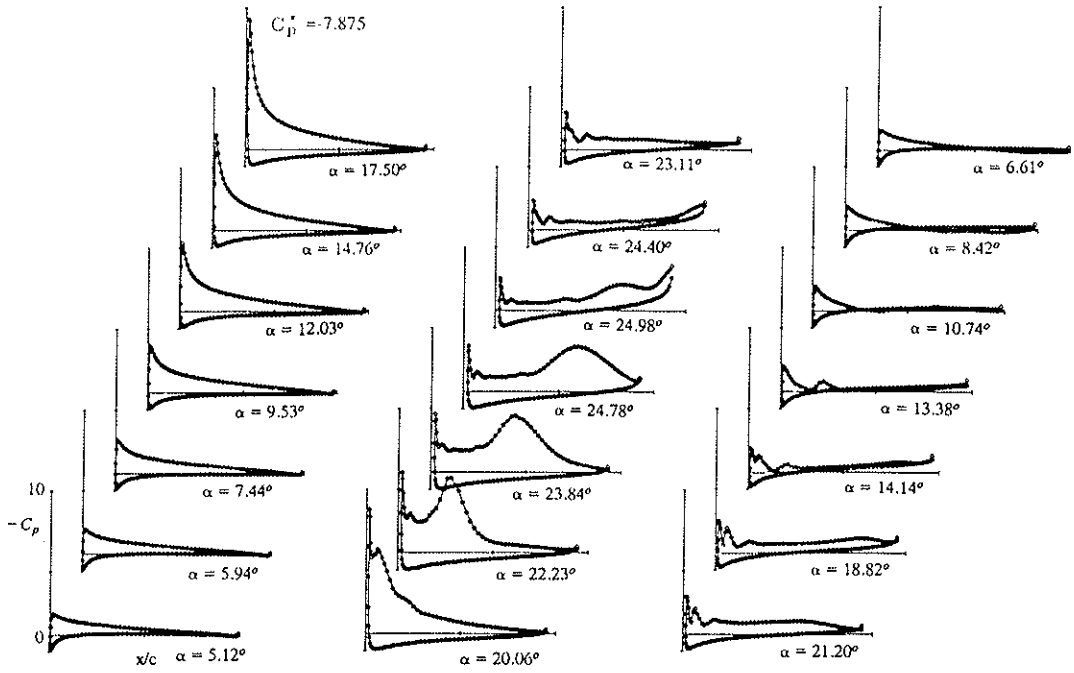

Fig. 4 Instantaneous Surface Pressure Distribution
NACA0012, $M_\infty = 0.283$, Re = 3.45×10^6, $\alpha = \alpha_0 + \alpha_m \sin(2M_\infty k\tau)$, $\alpha_0 = 15^o$, $\alpha_m = 10^o$, k=0.151

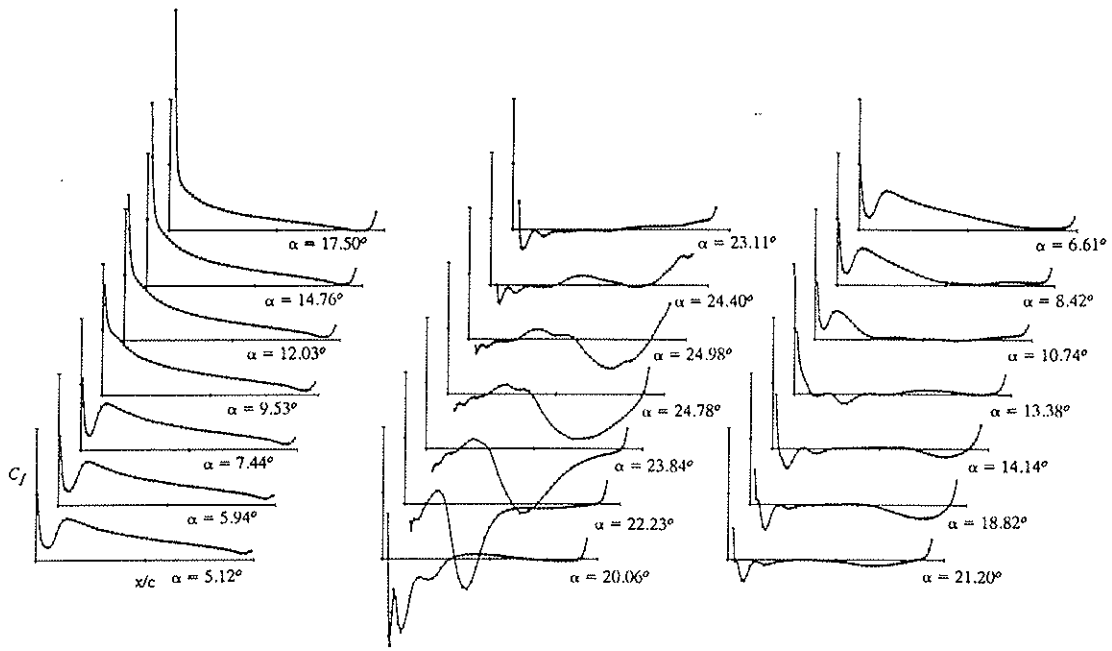

Fig. 5 Instantaneous Upper Surface Shear Stress Distribution
NACA0012, $M_\infty = 0.283$, Re = 3.45×10^6, $\alpha = \alpha_0 + \alpha_m \sin(2M_\infty k\tau)$, $\alpha_0 = 15^o$, $\alpha_m = 10^o$, k=0.151

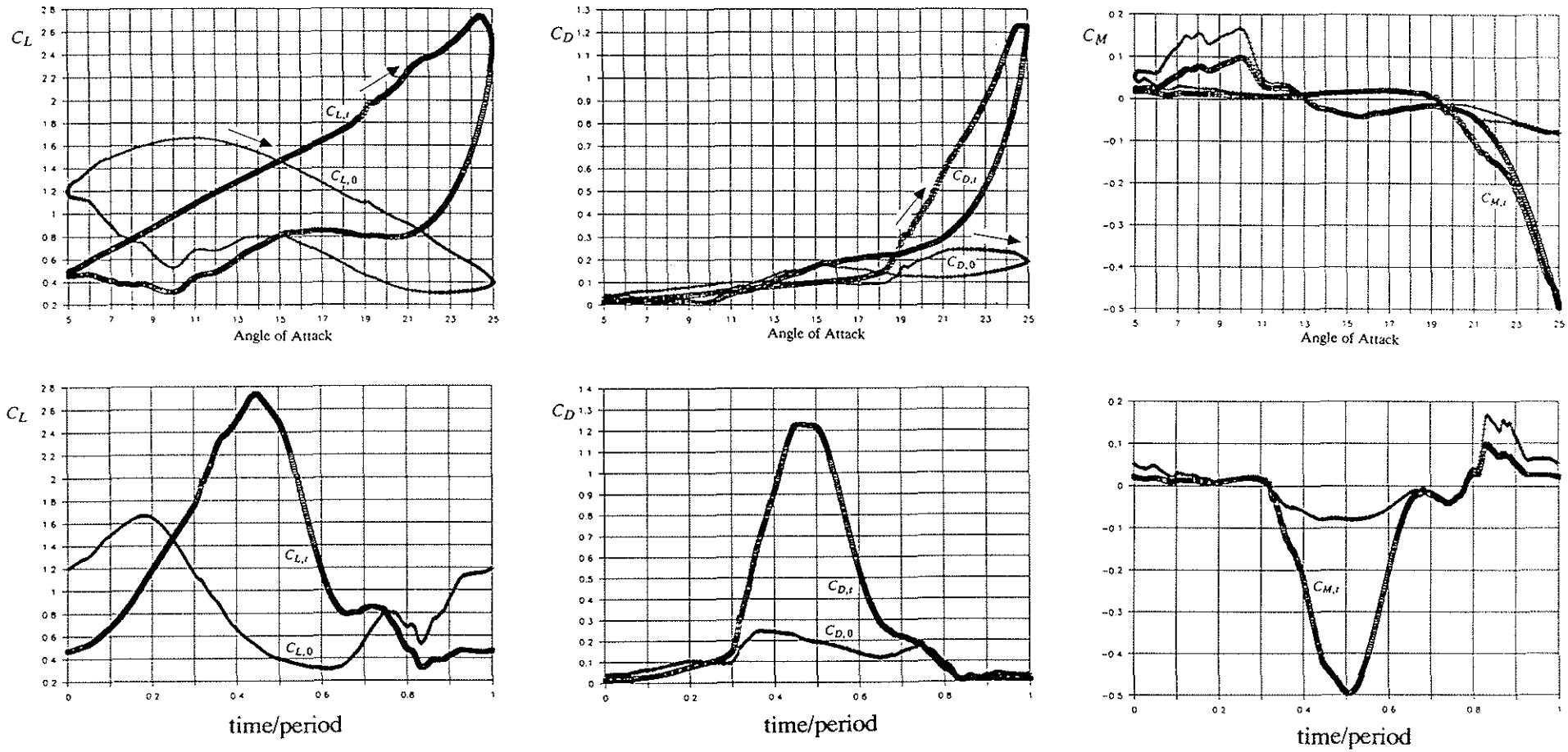

(a) Lift (b) Drag (c) Pitching Moment

Fig. 6 Aerodynamic Loads for Combind Velocity/Angle of Attack Oscillation
NACA0012, Re = 3.45×10^6, $M = M_0 - M_m\sin(2M_0k\tau)$, $M_0 = 0.283$, $M_m = 0.17$,
$\alpha = \alpha_0 + \alpha_m\sin(2M_\infty k\tau)$, $\alpha_0 = 15^o$, $\alpha_m = 10^o$, k=0.151